J. Fluid Mech. (1988), *vol.* 191, *pp.* 465–480
Printed in Great Britain

Vortex pairing and resonant wave interactions in a stratified free shear layer

By D. A. COLLINS† AND S. A. MASLOWE
Department of Mathematics and Statistics, McGill University, Montreal, PQ, H3A 2K6, Canada

(Received 27 March 1987 and in revised form 19 October 1987)

In a previous study using finite-amplitude techniques (Maslowe 1977), a strong instability mechanism was discovered that takes effect at the Richardson numbers consistent with turbulence observations in the atmosphere and oceans. The mechanism involves second harmonic resonance of two neutral or nearly neutral modes at a Richardson number of roughly 0.22. In the present investigation, the nonlinear Boussinesq equations have been solved numerically to further explore this instability and to assess the limits of validity of the theory. Qualitative agreement between the theory and numerical simulations was satisfactory as the most significant numerical results were predicted by the theory. In particular, the wave interaction leads to impressive instabilities at Richardson numbers large enough that a single linearly unstable wave would amplify only weakly. At a Richardson number of 0.14, for example, the saturation amplitude of the long wave in the two-wave interacting case was 15 times as large as the amplitude of the linearly most unstable wave (evolving by itself) at the same Richardson number.

1. Introduction

The stability theory of stratified shear flows has important geophysical applications as well as intriguing mathematical complexities. It is well known that there exist regions both in the atmosphere (the tropopause) and the oceans (thermoclines) where substantial shears are accompanied by stable density stratification. These mixing layers are often sites of considerable turbulence which is widely believed to be the outcome of shear flow instability. The term 'Kelvin–Helmholtz instability' is often employed, somewhat loosely, to describe this phenomenon which, according to inviscid linear stability theory, can occur only if $J(y)$, the local Richardson number, is somewhere less than $\frac{1}{4}$ (see, e.g. Drazin & Reid 1981). Laboratory studies tend to support the linear stability criterion, but have been conducted at Reynolds numbers much smaller than those pertinent to the atmosphere. Atmospheric observations of large amplitude waves, on the other hand, have been reported in which J_0, the minimum value of J, is between $\frac{1}{4}$ and 1 (see, e.g. Metcalf & Atlas 1973).

Kelvin–Helmholtz billows can achieve substantial amplitudes (on the order of 1 km) and their observation by sensitive radars has stimulated a considerable interest in the subject. Concurrent measurements of the Richardson number (which, unfortunately, cannot be determined precisely) indicate that the regime $0.15 \leqslant J_0 \leqslant 0.30$ frequently coincides with such observations, and this has often been taken as a substantiation of linear theory. However, upon further reflection, the situation is not

† Present address: Computer Modelling Group, Calgary, Alberta T2L 2A6, Canada.

so clear-cut because the linear growth rate of an unstable perturbation is quite small even at $J_0 = 0.15$ and seems incompatible with the spectacular billows reported, for example, in Browning (1971) and Hardy, Reed & Mather (1973). Moreover, viscosity and non-parallel effects reduce the linear growth rates from their inviscid values.

Given these circumstances, it is natural to search for nonlinear mechanisms that enhance the growth rates of unstable waves and/or suggest ways that instability can occur in flows that are stable on a linear basis. This search can be accomplished either by perturbation methods or by numerical solution of the full nonlinear Boussinesq equations. The numerical results presented here were obtained as the outcome of an attack on both fronts; the finite-amplitude theory provided guidance in the choice of initial perturbations as well as a framework in which to interpret the results.

The finite-amplitude study most pertinent to the present discussion was outlined in Maslowe (1977). Following an earlier suggestion by Kelly (1968), a perturbation was considered consisting of two resonantly interacting neutral modes in a mixing layer with velocity and density profiles $\bar{u} = \tanh y$ and $\bar{\rho} = \exp(-\beta \tanh y)$. It was found that the amplitudes of the two modes evolve according to the equations

$$\frac{\mathrm{d}A_1}{\mathrm{d}\tau} = \gamma_1 A_1^* A_2, \quad \frac{\mathrm{d}A_2}{\mathrm{d}\tau} = \gamma_2 A_1^2, \tag{1.1}$$

where $\tau = \epsilon t$ is a slow timescale, ϵ is an amplitude parameter and * denotes the complex conjugate. For the specific case considered, γ_1 and γ_2 were found to be each real and of the same sign, from which it is shown below that both waves can amplify by extracting energy from the mean flow. Because the amplification takes place on a faster timescale than in the weakly nonlinear theory for a single mode (ϵt *vs* $\epsilon^2 t$), this instability mechanism can be quite powerful, as suggested earlier by Kelly (1968). Further support for this conclusion is provided from numerical computations demonstrating that γ_1 and γ_2 can be quite large. The latter result is undoubtedly due to the presence of a critical layer, its role having been underlined in the boundary-layer case in a recent monograph by Craik (1985).

It is informative to rewrite (1.1) in terms of the real amplitude and phase denoted a and ϕ, respectively, where $A = \frac{1}{2}a\mathrm{e}^{-\mathrm{i}\phi}$ and $A^* = \frac{1}{2}a\mathrm{e}^{\mathrm{i}\phi}$. Equations (1.1) become

$$\mathrm{d}a_1/\mathrm{d}\tau = \tfrac{1}{2}\gamma_1 a_1 a_2 \cos\theta, \quad \mathrm{d}a_2/\mathrm{d}\tau = \tfrac{1}{2}\gamma_2 a_1^2 \cos\theta, \tag{1.2a,b}$$

$$\mathrm{d}\phi_1/\mathrm{d}\tau = -\tfrac{1}{2}\gamma_1 a_2 \sin\theta, \quad a_2\,\mathrm{d}\phi_2/\mathrm{d}\tau = \tfrac{1}{2}\gamma_2 a_1^2 \sin\theta, \tag{1.2c,d}$$

where, in studies of second harmonic resonance, $\theta = 2\phi_1 - \phi_2$ is termed the relative phase.

From (1.2a) and (1.2b), one can derive the energy integral

$$a_1^2 - (\gamma_1/\gamma_2)a_2^2 = E, \tag{1.3}$$

where E is a constant. This important result shows that both modes can amplify at the same time by extracting energy from the mean flow (recall that γ_1/γ_2 is positive). An integral involving the relative phase can also be derived from (1.2a)–(1.2d), namely

$$a_1^2 a_2 \sin\theta = L, \tag{1.4}$$

and, as noted by a referee, this can be combined with (1.2a) to yield

$$\mathrm{d}a_1^2/\mathrm{d}\tau = \gamma_1 L \cot\theta. \tag{1.5}$$

Finally, the relationships (1.2) and (1.3) can be used to derive the following equation for a_1^2:

$$\mathrm{d}^2 a_1^2/\mathrm{d}\tau^2 - \tfrac{1}{2}\gamma_1\gamma_2 a_1^2(3a_1^2 - 2E) = 0. \tag{1.6}$$

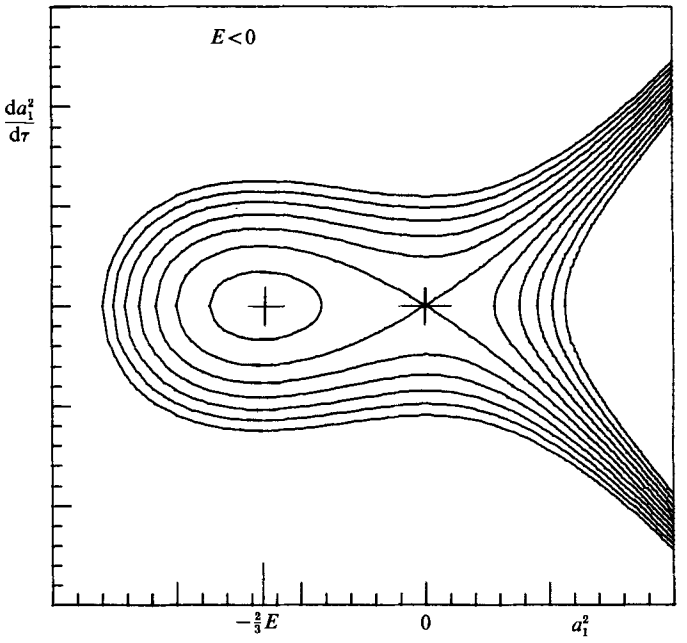

FIGURE 1. Phase plane trajectories for the long-wave amplitude.

A phase plane study of (1.6) shows that a_1^2 will generally become unbounded in time. This is true whether E is positive or negative, because the solution trajectories for which a_1 is real all lie to the right of a saddle point which is located at the origin when $E \leqslant 0$ or at $a_1^2 = \frac{2}{3}E$ if $E > 0$; the sketch in figure 1 corresponds with the latter case. The importance of the relative phase evident from (1.5) can also be seen clearly in the numerical calculations presented in figure 16 of Patnaik, Sherman & Corcos (1976). Their results were obtained by solving the Boussinesq equations with a disturbance consisting of a long and short wave having the wavenumbers $\alpha = 0.215$ and $\alpha = 0.43$. Other parameters were $J_0 = 0.07$, $Re = 50$ and $Pr = 0.72$, where Re and Pr denote the Reynolds and Prandtl numbers, respectively. Two cases were run, corresponding to different values of θ; the nature of the interaction was observed to be quite different in the two cases, although the long wave proved to be dominant each time.

Equations (1.1)–(1.6) also arise in the context of capillary–gravity waves, where experiments reported by McGoldrick (1970) strongly support the conclusions of the theory. The author states (p. 264) that 'the interaction process is so dramatic that it can be seen by eye'. This must be due not only to the relatively fast timescale, but also to the fact that the two-wave resonance requires only the longer wave to get started; the second harmonic is generated automatically by weak nonlinear effects. For capillary–gravity waves the process is one of energy-sharing so that $\gamma_1/\gamma_2 < 0$†. Hence, there is reason to expect even more dramatic results in the case where shear is available as an energy source for both waves.

There is no doubt that the resonance described above is related to the vortex-pairing process observed to occur in homogeneous mixing layers. Numerical

† When an external stream is present, Nayfeh (1973) has shown that for a certain range of velocities spatial amplification of both waves is possible. This appears to be a group velocity effect related only indirectly to the instability studied here.

simulations by Riley & Metcalfe (1980), for example, illustrate convincingly that the two-wave perturbation describes well the sequence of events observed experimentally. Their results also demonstrate the importance of the relative phase; in fact, it is only when $|\theta| = \frac{1}{2}\pi$ that pairing fails to occur. It would be claiming too much, however, to say that the theory outlined above is directly relevant to transition in homogenous free shear layers, because the wavenumbers involved are too far away from the neutral value (e.g. $\alpha_n = 0.895$ when $Re = 50$). The application to stratified shear layers is more promising because linear growth rates are smaller, and the range of unstable wave numbers decreases with increasing J_0, vanishing entirely at $J_0 = \frac{1}{4}$. By adding linear amplification terms to (1.1), a meaningful portion of the (J_0, α)-space is accessible to the perturbation theory.

Given the restrictions of the theory to small amplitudes and to wavenumbers that are not necessarily the fastest growing, the present numerical investigation was undertaken to extend the earlier results and answer questions that were raised by both finite-amplitude theories and previous numerical studies. For example, one may wonder if it is of any interest to examine the interaction of neutral modes, as discussed above, when a band of linearly unstable waves exists at the same Richardson number? Section 3 deals with two-wave interaction cases and results presented there show, in fact, that the shorter of the two neutral modes can grow at a rate roughly 5 times that of the linearly most unstable wave. A second question pursued in the same section pertains to the effect of stratification on the vortex-pairing process, i.e. what qualitative features of the interaction change as J_0 is increased and what is the maximum value for which pairing can occur?

Although this paper does not provide definitive answers to these questions, there are some surprising results clearly indicating that two-wave interactions are significant at moderate values of the Richardson number. They may partially explain, for example, the variability in observed wavelengths reported by meteorologists and the tendency noted by Greene & Hooke (1979) toward longer waves *vis-à-vis* the most amplified wave of linear theory. Further discussion of our results is deferred until §4 so that the governing equations can be presented, followed by a description of the numerical methods used to solve them.

2. Formulation and numerical procedures

After employing the Boussinesq approximation, the non-dimensional equations of motion can be written

$$\zeta_t + \Psi_y \zeta_x - \Psi_x \zeta_y + \frac{J_0}{\beta}\rho_x = \frac{1}{Re}\nabla^2\zeta, \tag{2.1}$$

and

$$\rho_t + \Psi_y \rho_x - \Psi_x \rho_y = \frac{1}{Re\,Pr}\nabla^2\rho, \tag{2.2}$$

where the velocity components are related to the stream function by $(u, v) = (\Psi_y, -\Psi_x)$, the vorticity $\zeta = -\nabla^2\Psi$ and ρ is the density. The dimensionless parameters which emerge are the Reynolds and Prandtl numbers, Re and Pr, as well as J_0, the minimum value of the local Richardson number $J(y)$, whereas

$$\beta \equiv -\mathrm{d}(\log\bar{\rho})/\mathrm{d}y,$$

evaluated at $y = 0$ which, for our model, is also the level at which $J(y) = J_0$. These scalings are standard in shear-layer stability investigations and correspond, for example, with the sketch in figure 1 of Patnaik *et al.*

Equations (2.1) and (2.2) were solved in the finite rectangular domain $0 \leqslant x \leqslant \lambda$, $-3\lambda/2\pi \leqslant y \leqslant 3\lambda/2\pi$, where λ is the wavelength of the disturbance and the solution is periodic in x. For the wave interaction cases, λ is the wavelength of the longer of the two waves. The conditions imposed along the horizontal computational boundaries located at $y = \pm 3\lambda/2\pi$ approximated exponential decay of the perturbation and tests were made to ensure that the results were not sensitive to the boundary location.

As the undisturbed velocity and density profiles in our study, we employed the Hølmboe model of a mixing layer, namely, $\bar{u} = \tanh y$ and $\bar{\rho} = \exp(-\beta \tanh y)$. Although this is not an exact solution of the Boussinesq equations, it is known to approximate experimentally measured profiles accurately as found, for example, by Scotti & Corcos (1972) and Davey & Roshko (1972). The major advantage of this model is that the inviscid neutral solution is known in closed-form; moreover, numerical codes were available to us for solving the linear diffusive stability problem, namely, those used by Maslowe & Thompson (1971), and these codes were employed to provide initial conditions in the numerical simulations. Because inviscid neutral modes are singular, it was essential that dissipative effects be included.

The governing partial differential equations were solved using the pseudospectral method as described, for example, by Gottlieb & Orszag (1977). The use of this method is now so widespread in geophysical and engineering applications that only a sketch of our particular implementation seems necessary here. Briefly, the vorticity and density in (2.1) and (2.2) were represented by the series

$$\zeta = \bar{\zeta}(y) + \sum_m \sum_n a_{mn} \exp\{\mathrm{i}(m\alpha x + n\mu y)\}, \tag{2.3}$$

and

$$\rho = \bar{\rho}(y) + \sum_m \sum_n b_{mn} \exp\{\mathrm{i}(m\alpha x + n\mu y)\}, \tag{2.4}$$

where $\alpha = \pi/L_x$ and $\mu = \pi/L_y$ with L_x and L_y being half the domain size in the horizontal and vertical directions, respectively. By separating ζ and ρ into periodic and non-periodic components in this way, Gibbs phenomenon which adversely affects the convergence of the series is kept to a minimum.

Pseudospectral (as opposed to spectral) methods employ collocation to determine the coefficients of the series in (2.3) and (2.4). We denote the number of collocation points in the horizontal by $n1$ and the number in the vertical by $n2$. The spatial derivatives in (2.1) and (2.2) were calculated using term-by-term differentiation in Fourier space and then transformed into physical space where nonlinear terms were calculated pointwise. Time differencing was accomplished by employing the explicit second-order Adams–Bashforth scheme with the first few (small) steps computed using Euler's method. It was found that the Adams–Bashforth method was more stable and somewhat faster than the more widely used leapfrog differencing.

As noted earlier, weakly nonlinear theories provide a framework within which the results of numerical simulations can be most usefully interpreted. This requires that amplitudes in the numerical study be defined in such a way that identification is feasible with the quantities $A_i(\tau)$ appearing in the theory. For simplicity, let us first consider a perturbation consisting of a single mode. In linear theory, the stream function can be written

$$\Psi(x, y, t) = \int^y \bar{u}(s)\,\mathrm{d}s + \epsilon\{A(t)\,\phi(y) + *\}, \tag{2.5}$$

where ϵ is a dimensionless amplitude parameter related to the disturbance energy as follows.

In accordance with (2.5), the perturbation kinetic energy to $O(\epsilon^2)$ is given by

$$E(t) = \epsilon^2|A|^2 \int_{-\infty}^{\infty} (|\phi'|^2 + \alpha^2|\phi|^2)\,\mathrm{d}y. \tag{2.6}$$

The integral in (2.6) is equal to $\frac{8}{3}$ in the case of the inviscid, unstratified neutral mode $\phi = \operatorname{sech} y$, $\alpha = 1$. Consistent with this normalization which we employed for ϕ in general, $A(0)$ was set equal to $(\frac{3}{8})^{\frac{1}{2}}$; in the two-mode runs, this convention was used for the fundamental mode, with the amplitude of the subharmonic varying in different cases.

Representing now the eigenfunction by a Fourier series, we have

$$\phi(y) = \sum_{n=-\frac{1}{2}N2}^{\frac{1}{2}N2-1} p_n\, \mathrm{e}^{\mathrm{i}n\mu y}. \tag{2.7}$$

In our numerical code, the counterpart of (2.5) is written

$$\Psi = \int^y \bar{u}(s)\,\mathrm{d}s + \sum_{m=-\frac{1}{2}N1}^{\frac{1}{2}N1-1} \sum_{n=-\frac{1}{2}N2}^{\frac{1}{2}N2-1} \mathrm{d}_{mn}(t) \exp\{\mathrm{i}(m\alpha x + n\mu y)\}, \tag{2.8}$$

which, by comparison with (2.7), yields

$$A(t) \approx \sum_{n=-\frac{1}{2}N2}^{\frac{1}{2}N2-1} \mathrm{d}_{1n}(t)\, p_n^* \Big/ \sum_{n=-\frac{1}{2}N2}^{\frac{1}{2}N1-1} |p_n|^2. \tag{2.9}$$

This amplitude differs from the $A(t)$ of weakly nonlinear stability theories, where $A(t)$ is the first term in a series in powers of ϵ (see e.g. Stuart 1971). However, for a single mode the next term of the series is zero and so we may expect to be able to make a reasonable comparison with linear theory for small times as a check on accuracy. This is not as easily accomplished with finite-difference methods, as discussed by Patnaik *et al.* because there the kinetic energy, which is employed as a measure of amplification, includes all the higher harmonics in x.

We have made such comparisons and find, for example, a deviation of only about 1% from the αc_{i} of linear theory after 8 dimensionless time units for the fastest growing mode at the following parametric values: $J_0 = 0.07$, $\alpha = 0.45$, $Re = 200$, $Pr = 0.72$ and $\epsilon = 0.01$ to 0.05. The agreement was not as close for neutral modes, but was still satisfactory. For details of these comparisons and further discussion of the numerical procedures employed see Collins (1982). One further remark, however, about pseudospectral methods is that aliasing errors inherent in the method are evident if the energy spectrum is graphed as a function of wavenumber. A marked increase in the high wavenumbers (small scales) occurs when numerical instability is present, in which case the number of modes must be increased and/or the timestep decreased. This monitoring procedure was followed in all cases.

3. Numerical results

We have run a number of single mode simulations at Reynolds numbers as high as 600 in order to compare the results with various asymptotic theories. Brown, Rosen & Maslowe (1981), for example, in a weakly nonlinear analysis of the Hølmboe mixing layer found a strong dependence on Prandtl number of the Landau constant. A more thorough investigation by Churilov & Shukhman (1987) produced the same trend and confirmed, in particular, that the Landau constant is negative (nonlinear

effects are stabilizing) when $Pr < 1$. Surprisingly, a strong variation with Pr was not observed in our simulations (some possible explanations are proposed in §4) and, consequently, the matter was not pursued.

More satisfactory comparisons were achieved, however, with the nonlinear critical-layer theory, where the numerically computed flow structure near saturation bears a strong resemblance to the theoretical model, including the presence of the thin diffusive 'braids' predicted by the theory. A typical pattern for the isopycnic (constant-density) contours in the critical layer is illustrated in figure 5 of the recent survey article by Maslowe (1986); this case corresponds to the parameter values $J_0 = 0.10$, $Re = 200$, $Pr = 0.72$ and $\alpha = 0.44$.

According to the nonlinear critical-layer analysis for stratified flows, all harmonics of the fundamental disturbance mode are the same order of magnitude in the critical layer. A consequence for numerical studies, borne out by our experience, is that many modes must be employed to resolve properly the complex flow occurring at high Reynolds numbers, especially when diffusive layers are present. As discussed by Curry *et al.* (1984), the use of an insufficient number of modes in such circumstances will produce spurious chaos. For the highest Reynolds numbers we considered, a 128×128 grid was required.

For the two-mode interactions, which are the focal point of this article, it was observed that the dynamics are essentially inviscid at $Re = 200$ so that value, along with $Pr = 0.72$, was employed in the computations whose results are presented below. It was found that the minimum resolution requirement was 32 Fourier modes in x and 64 in y with a timestep of 0.0625. No dramatic changes with Reynolds number were noted for $Re > 200$ and so we conclude that the dominant parameters governing the interaction are the Richardson number, wavenumber, amplitude ratios and the relative phase.

3.1. *Neutral modes*

Figure 2 indicates the stability on a linear basis of the individual modes involved in our computations by noting their position relative to the neutral curve and to the locus of most amplified wavenumbers. Due to the symmetry of Hølmboe's flow, $c_r = 0$ in all cases and the resonance condition therefore is simply that the wavenumbers be in a 2:1 ratio.

The case corresponding exactly with the theory outlined earlier, i.e. equations (1.1)–(1.5), coincides with the Richardson number $J_0 = 0.217$ when $Re = 200$. Although the instability in this case did not prove to be as substantial as suggested by the finite-amplitude theory, the results were none the less interesting. In particular, the initial growth rate for the short wave (for which $\alpha = 0.642$) considerably exceeded that of the linearly most unstable wave (whose $\alpha c_i = 0.025$), as shown in figure 3. On the other hand, the increase in saturation amplitude was less dramatic because the linearly most amplified wave grows until $t = 24.5$, whereas the resonant neutral mode stops growing at $t = 5.6$; its amplitude at that point is 18% larger than the maximum achieved by the linearly most unstable wave.

The initial conditions leading to relatively rapid growth of the short wave included setting $a_1(0) = 30a_2(0)$. In such a case, the process might be described as linear instability of an initially periodic flow consisting of the mixing layer and the longer wave because the amplitude of the long wave remained relatively constant during the interaction. This situation is reminiscent of Kelly's (1967) analysis of subharmonic instability in a homogeneous mixing layer with one important difference – in the unstratified case, it is the long wave which amplifies and the short one is taken to be periodic.

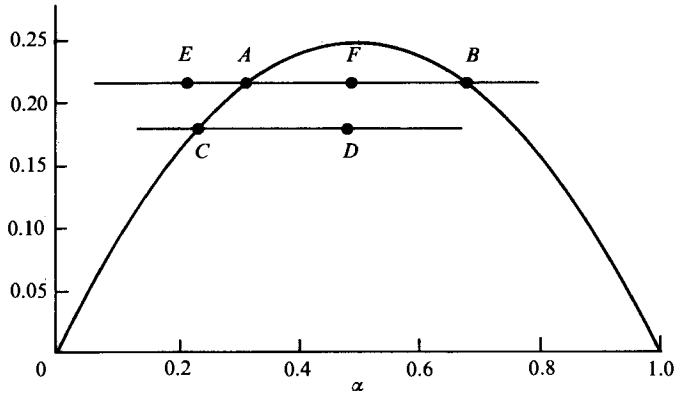

FIGURE 2. Linear stability boundary for Hølmboe's flow and location of pairs of resonantly interacting modes discussed in §3.1 (A, B), §3.2 (C, D) and §4 (E,F).

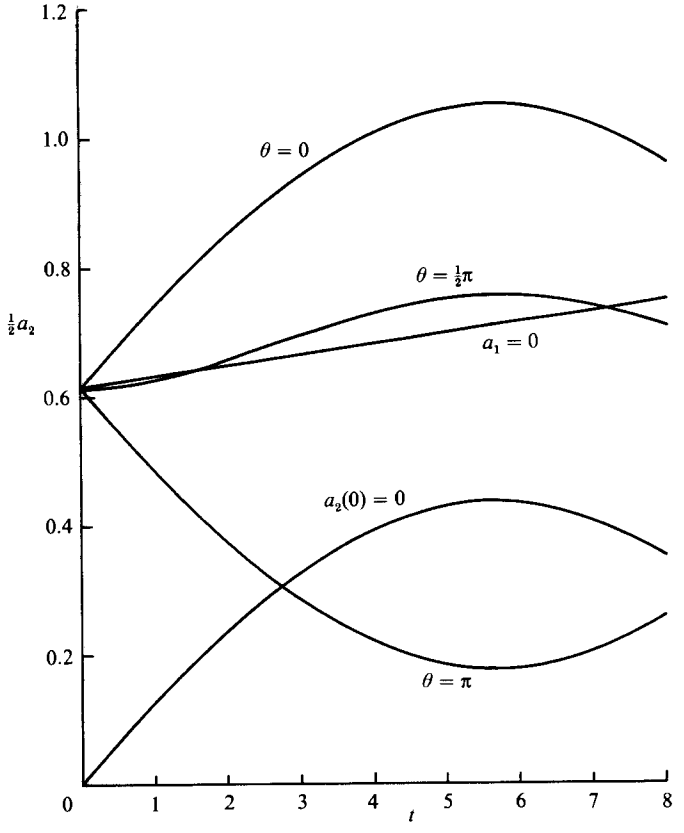

FIGURE 3. Amplitude evolution of short wave $a_2(t)$ in the case of two interacting neutral modes and dependence on initial relative phase θ; $J_0 = 0.217$, $Re = 200$, $Pr = 0.72$, $\epsilon = 0.004$, $\alpha_1 = 0.321$, $\alpha_2 = 0.642$ and $a_1(0) = 30a_2(0)$, except in the cases $a_2(0) = 0$ and $a_1 = 0$ (long wave absent).

Our failure to find initial conditions leading to amplification of the long wave at $J_0 = 0.217$ is surprising in light of the known results for homogeneous mixing layers (see Ho & Huerre 1984 for a review). Moreover, the pairing simulations of Patnaik *et al.* at $J_0 = 0.07$ illustrate that a slight stratification does not eliminate this process. On the other hand, our results do make it clear that notions about 'vortex pairing'

must be considerably altered when the stratification is moderate, a point that will be taken up again in §3.3. First, however, some brief further observations are made about interacting neutral modes.

When θ, the relative phase, is equal to π, figure 3 indicates that the short wave at first decays but, eventually, amplifies at a rate approaching that of the most favourable case, namely, $\theta = 0$. This behaviour is completely in accordance with the phase plane diagram in figure 1, corresponding with a trajectory to the right of the saddle point, but starting with a negative value of $\mathrm{d}a^2/\mathrm{d}\tau$. A second, perhaps more significant, point of agreement between numerical simulation and resonant interaction theory is that the short wave will amplify even if it is not present initially (cf. curve in figure 3 originating at the origin) because it is generated by self-interaction of the long wave.

Despite the at least academic interest of these results, the outcome of the interacting neutral mode simulations was judged as disappointing because of the unimpressive saturation amplitudes. Significant progress was achieved, however, by a slight lowering of the Richardson number, as described below.

3.2. *Interaction of a neutral mode with the most amplified wave*

The value $J_0 = 0.174$ is special in that the second harmonic of the longer neutral mode (i.e. $\alpha = 0.225$) is the fastest growing wave of linearized stability theory. Hence, we consider the interaction of these two waves (see figure 2) and expect the resonance theory to apply because, for the unstable wave, αc_i is not large nor is the difference between J_0 and its neutral value at $\alpha = 0.45$.

Again, the initial amplitudes were related by $a_1(0) = 30a_2(0)$ and, although we do not present a plot of $a_1(t)$, we note that some amplification of the 'neutral' mode occurred. The temporal variation of a_2 is shown in figure 4 and the strong dependence on the relative phase is evident, as in the just-discussed case of two neutral modes. Most noteworthy is the substantial enhancement of the initial amplification rate *vis-à-vis* the single-wave case but, again, the increase in saturation amplitude is not commensurate with the factor of five magnification of the initial coefficient of amplification. This would seem to indicate that higher-order terms in the amplitude evolution equations are stabilizing. To obtain large saturation amplitudes, the most favourable configuration appears to be two linearly unstable waves interacting in such a way that the longer one essentially dominates, and we now proceed to that case.

3.3. *The effect of stratification on vortex pairing*

Results are presented here concerning interactions between the most unstable wave on a linear basis and its subharmonic for the range of Richardson numbers $0.07 \leqslant J_0 \leqslant 0.14$. The Reynolds number was fixed at $Re = 200$ and we begin with a comparison of the evolution at $J_0 = 0.07$ with the corresponding results at $Re = 50$, i.e. the case considered by Patnaik *et al.*

The isopycnic lines illustrated in figure 5 describe a process of vortex roll-up and subsequent coalescence that clearly is similar to that occurring in homogeneous mixing layers. The rotation of the two vortex cores prior to coalescence seems to be much more energetic at $Re = 200$ than at $Re = 50$ (cf. figure 16 of Patnaik *et al.*) and the saturation amplitude is greater by 34%. Also of note is a significant presence of the short-wave component ($a_2 \approx 0.35a_1$) at large times even though visually one has the impression that the long wave is totally dominant. Thus, it may be more appropriate to describe the process as one of wave interaction instead of employing the language of vortex dynamics, despite its descriptive appeal.

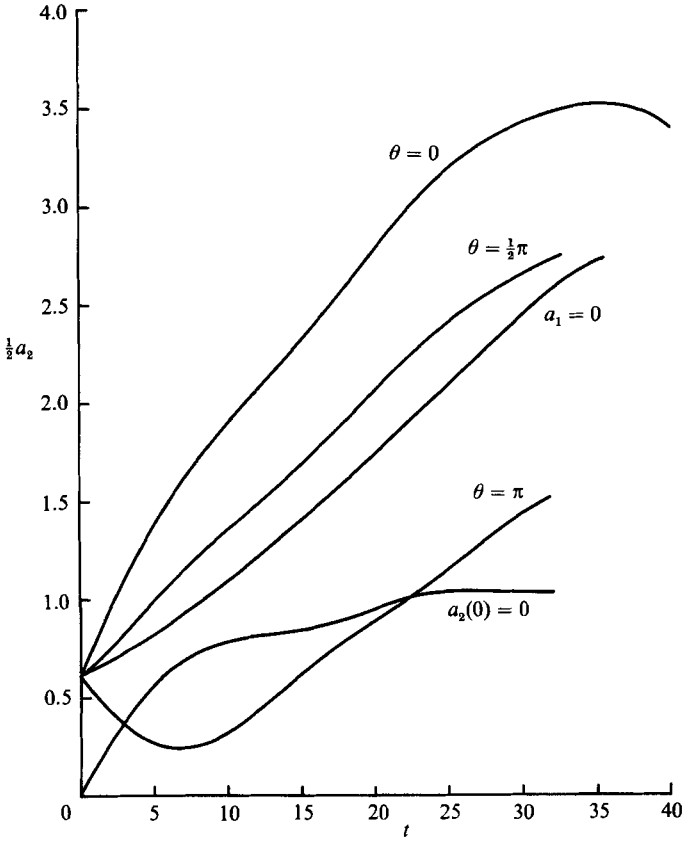

FIGURE 4. Amplitude evolution of linearly most unstable wave $a_2(t)$ with and without its (neutral) subharmonic and dependence on initial relative phase θ in the first case; $J_0 = 0.174$, $Re = 200$, $Pr = 0.72$, $\epsilon = 0.004$, $\alpha_1 = 0.225$, $\alpha_2 = 0.45$ and $a_1(0) = 30a_2(0)$, except when $a_2(0) = 0$ and $a_1 = 0$.

Additional simulations were made at progressively larger Richardson numbers in order to assess the effect of stable stratification on the process described above. Some of these data are summarized in table 1. From a visual standpoint, a limiting case is reached at $J_0 = 0.14$ wherein the left vortex rises only slightly while a corresponding slight descent of the right vortex occurs, as seen in figure 6(*b*). None the less, the eventual merging of the two leads to a substantial amplification of the 'billow' which is apparent in figure 6(*c*). In fact, the maximum amplitude achieved by the long wave is on the order of 15 times that of the linearly most unstable wave amplifying alone.

The latter result is the most promising one we have obtained in terms of explaining the atmospheric observations of large waves at Richardson numbers too large for linear instability to be responsible. Moreover, there is the possibility of achieving further progress by considering other interactions such as those involving oblique waves. Even in the context of two-dimensional perturbations, Corcos & Sherman (1984) find that the addition of a second subharmonic leads to further amplification in the unstratified case via a second pairing. However, a second subharmonic would be linearly damped in our stratified model and, while such a wave triad can occur, it is unlikely that such events arise frequently in practice.

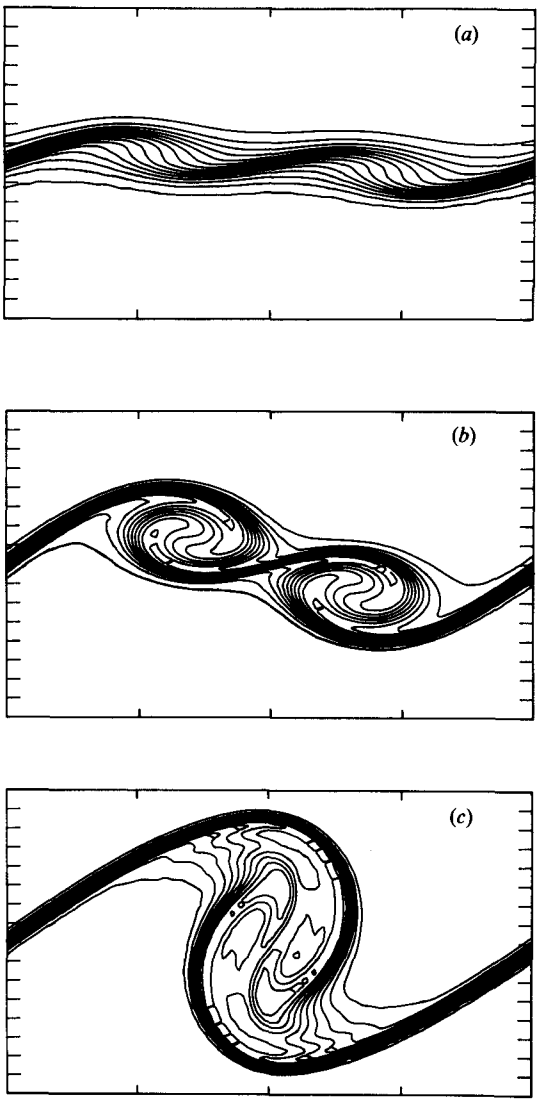

FIGURE 5. Temporal evolution of isopycnic (constant-density) contours in the case $J_0 = 0.07$, $Re = 200$, $\alpha_1 = 0.215$, $\alpha_2 = 0.43$: (*a*) $t = 16$; (*b*) 32; (*c*) 48.

4. Concluding remarks

A principal objective of this investigation was to learn whether a perturbation consisting of two resonantly interacting normal modes could produce large-amplitude Kelvin–Helmholtz billows at Richardson numbers in the range $0.10 \leqslant J_0 \leqslant 0.25$. Linear growth rates, as discussed in §1, are too small at such values of J_0 to explain reported observations in the atmosphere of waves with enormous amplitudes. We have, in fact, succeeded in demonstrating that resonance does lead to significant enhancement of saturation amplitudes in the lower part of this range, say $0.10 \leqslant J_0 < 0.15$. Results obtained at larger values of J_0, however, were inconclusive because those instabilities which amplified most impressively initially often equilibrated relatively rapidly. Some further discussion of this is given below, but first, we take

Re	J_0	$a_{1_{max}}$	t_{max}
50	0.07	24.5	46
200	0.07	32.8	41.5
200	0.10	26.1	46.3
200	0.12	22.4	48.3
200	0.14	18.4	63.6

TABLE 1. Maximum amplitude of subharmonic and time at which it was reached for two interacting unstable modes. In all of these cases, $a_1(0) = 2a_2(0)$, $\theta = 0$ and $Pr = 0.72$. A 64×128 grid was used for the $Re = 200$ simulations.

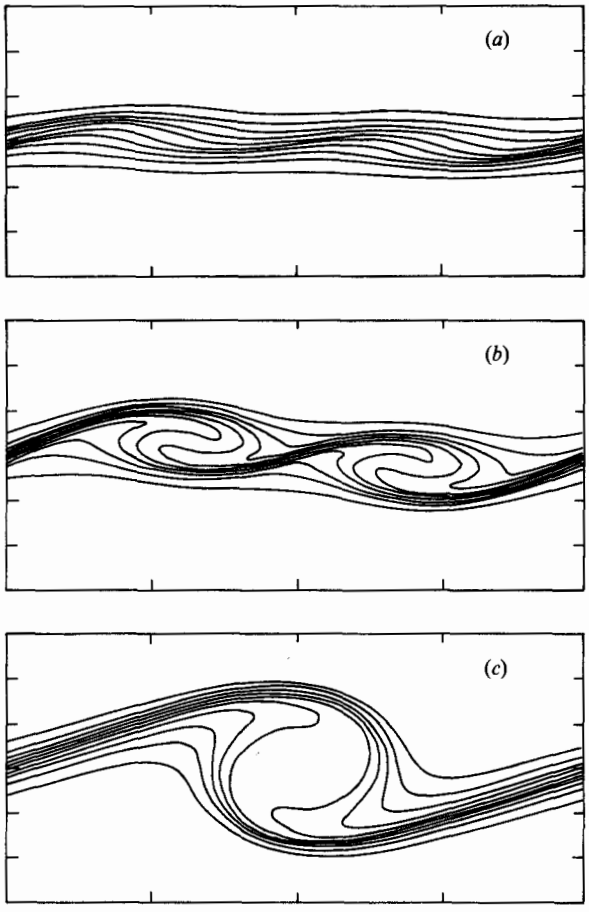

FIGURE 6. Temporal evolution of isopycnic contours in the case $J_0 = 0.14$, $Re = 200$, $\alpha_1 = 0.23$, $\alpha_2 = 0.46$: (a) $t = 16$; (b) 32; (c) 56.

up a topic about which more can be said, namely, the dominant wavelength of observed disturbances.

There was a period of time dating from the publication by Woods (1968) of his internal wave measurements in the Mediterranean when instabilities observed in the atmosphere and oceans were often reported to have a wavelength 7.5 times the

thickness of the shear layer in which they propagated. This figure corresponds to the fastest growing wave in the three-layer stratified flow model studied by Miles & Howard (1964). Our results, however, render any claim about the generality of the forementioned figure highly suspect, particularly at values of $J_0 \leqslant 0.15$, where modal interactions favour the transfer of energy to longer waves.

Even in the case of a single mode, Patnaik *et al.* found that long waves at small values of J_0, despite not having the largest amplification rate initially, eventually attained more impressive dimensions than shorter waves. The case $J_0 = 0.03$, $Re = 50$ was selected to illustrate the dependence on α (see their figure 9) with isopycnic contours presented at $\alpha = 0.2$, 0.43 and 0.7. These results can be explained, in part, by means of the second harmonic resonance theory if we recall that the harmonic of the fundamental perturbation will always be generated even if it is not present initially. In the case $\alpha = 0.2$, the second harmonic of the fundamental mode corresponds to $\alpha = 0.4$, a wavenumber for which αc_i is large, and consequently a strong interaction will ensue once the $\alpha = 0.4$ mode achieves a finite amplitude. By contrast, the second harmonic of the linearly most amplified wave is, at $Re = 50$, a nearly neutral mode; it will always remain small thus precluding an interaction of the sort treated in this study.

Returning now to the question of observed wavenumbers, near the critical value of J_0 there may be reason to expect natural instabilities to have the wavenumber of the linearly most amplified disturbance. Although in §3.1 and §3.2 we presented results indicating a bias toward short waves, the ratio of initial amplitudes of the two modes in those cases was specially chosen. The resulting instabilities illustrated interesting possibilities, but they may not occur often in the natural environment. We have made some additional computations at $J_0 = 0.217$ showing that the growth rate of the most amplified disturbance (point F in figure 2) can be increased substantially by the presence of a linearly damped subharmonic (point E), so many outcomes are possible depending upon initial conditions.

Greene & Hooke (1979) report a study of 35 atmospheric events in which they find considerable variability of wavelengths but, none the less, there is a tendency toward long waves, sometimes 10–20 times the shear-layer thickness. These data probably reflect the real situation and we conjecture that nonlinear interactions account for some of the variability in wavelengths, as well as the prevalence of long waves. However, real atmospheric wind and temperature profiles sometimes differ considerably from the models employed in stability calculations and that must also be taken into account.

At several points in this article, we have underlined the importance of finite-amplitude methods in the interpretation of numerical experiments and in providing guidance as to the choice of potentially interesting initial conditions. No quantitative comparisons are reported here, however, because those that we have made indicate that neglected higher-order terms in (1.2) are significant. In particular, the distortion of the mean flow appears at the next order and this effect, which is stabilizing, is clearly important because the mean shear is the energy source permitting both waves to amplify in the resonant cases. However, other terms arise at the same order and their sign cannot be predicted. The relevant amplitude equations to the order required have been derived by Usher & Craik (1975) for the case of resonant triads in a boundary layer. To formulate an equivalent analysis describing the two-mode interaction in a stratified free shear layer would be a formidable undertaking, but this is what must be done before a quantitative comparison can be made between resonance theory and numerical simulation.

In the present investigation, computations were made only for the Hølmboe model; however, the notions of vortex pairing and second harmonic resonance are pertinent to other shear flows and certain of these are now discussed. For example, a number of papers in meteorological journals have considered the same velocity profile as we have, $\bar{u} = \tanh y$, but with density profiles having non-zero stratification outside of the mixing layer. In such cases, a second class of modes (termed 'radiating') can occur which have eigenfunctions that are oscillatory rather than exponentially decaying as $|y| \to \infty$, i.e. they have a gravity wave nature. These radiating modes typically have much smaller linear growth rates than Kelvin–Helmholtz modes at the same value of J_0. The two studies discussed immediately below have an objective that differs from our own – they raise the question of whether, as a result of weak nonlinear interactions, radiating modes might play a more prominent role than linear theory suggests.

Davis & Peltier (1979) have considered the interaction between a radiating mode and a Kelvin–Helmholtz mode having twice its wavenumber. Their analysis, which differs in detail from that of Maslowe (1977), leads none the less to amplitude equations analogous to (1.1). At a Richardson number $J_0 = 0.125$, these authors find that the coefficients of the nonlinear terms have values such that substantial amplification of the radiating mode (which is nearly neutral on a linear basis) is possible. Fritts (1984), on the other hand, integrated the Boussinesq equations numerically and found that the 'pairing efficiency' was greatly reduced, compared with the Hølmboe density profile when $\bar{\rho} = \exp(-\beta y)$ and the long wave was of radiating type. The latter study treated only very small Richardson numbers, $0.025 \leqslant J_0 \leqslant 0.05$, and only 8 Fourier modes were used in the x-direction. Despite the limited resolution, one would expect these results to be qualitatively correct for a certain period of time given that the value $Re = 100$ employed in the computations was not excessively large.

Although the density profiles were not the same in these two studies, it is still surprising that such different conclusions were reached, and we offer some speculations that may partially explain these differences. First, while the proposal of Davis & Peltier is interesting and reasonable, their inviscid analysis ignores critical-layer effects which must surely alter the value of the interaction coefficients. It should be recalled that the critical-point singularity is stronger in stratified shear flows than in the homogeneous case, and careful consideration of the critical layer is essential (see e.g. Churilov & Shukhman 1987 or Maslowe 1986). In assessing the investigation of Fritts, on the other hand, the question is more one of choosing appropriate initial conditions and properly interpreting the results. For example, the author's definition of pairing efficiency is based on the ratio of the energy in the long wave to that in the short wave. However, efficient pairing may depend more on maximizing the energy transfer from the mean flow to *both* waves and, as noted in §3.3, there may remain a sizeable amount of energy in the short wave even after pairing. Clearly, the question of energy transfer to radiating modes is deserving of further study, particularly at the larger values of Richardson number most pertinent to the atmosphere.

Finally, we comment briefly on the effect of planetary rotation on vortex pairing in homogeneous mixing layers. The unstable, as well as neutral modes, of a $\tanh y$ shear layer on the β-plane are highly dispersive. Consequently, the necessary conditions for second harmonic resonance are not generally satisfied, and on that basis we expect that vortex pairing will diminish with increasing β. Laroche (1987) has recently investigated this question numerically by introducing a white-noise

perturbation containing all wavelengths compatible with his computational domain. In accordance with the foregoing considerations, he finds that pairing is rapidly suppressed even at values of β small enough to permit significant amplification of individual modes. These results will be submitted for publication in the near future.

The authors are indebted to Professors R. W. Metcalfe and S. A. Orszag for their expert advice relative to the development and utilization of our numerical code. We also thank Professor W. D. Thorpe for authorizing partial support of the McGill Computing Centre for the computations reported herein. Finally, we acknowledge the research support of the Natural Sciences and Engineering Research Council of Canada.

REFERENCES

BROWN, S. N., ROSEN, A. S. & MASLOWE, S. A. 1981 The evolution of a quasi-steady critical layer in a stratified viscous shear layer. *Proc. R. Soc. Lond.* A **375**, 271–293.

BROWNING, K. A. 1971 Structure of the atmosphere in the vicinity of large-amplitude Kelvin–Helmholtz billows. *Q. J. R. Met. Soc.* **97**, 283–299.

CHURILOV, S. M. & SHUKHMAN, I. G. 1987 Nonlinear stability of a stratified shear flow: a viscous critical layer. *J. Fluid Mech.* **180**, 1–20.

COLLINS, D. A. 1982 A numerical study of the stability of a stratified mixing layer. PhD thesis, McGill University.

CORCOS, G. M. & SHERMAN, F. S. 1984 The mixing layer: deterministic models of a turbulent flow. Part 1. Introduction and the two-dimensional flow. *J. Fluid Mech.* **139**, 29–65.

CRAIK, A. D. D. 1985 *Wave Interactions in Fluid Flows.* Cambridge University Press.

CURRY, J. H., HERRING, J. R., LONCARIC, J. & ORSZAG, S. A. 1984 Order and disorder in two- and three-dimensional Bénard convection. *J. Fluid Mech.* **147**, 1–38.

DAVEY, R. F. & ROSHKO, A. 1972 The effect of a density difference on shear-layer instability. *J. Fluid Mech.* **53**, 523–543.

DAVIS, P. A. & PELTIER, W. R. 1979 Some characteristics of the Kelvin–Helmholtz and resonant over-reflection modes of shear flow instability and of their interaction through vortex pairing. *J. Atmos. Sci.* **36**, 2394–2412.

DRAZIN, P. G. & REID, W. H. 1981 *Hydrodynamic Stability.* Cambridge University Press.

FRITTS, D. C. 1984 Shear excitation of atmospheric gravity waves: Part II. *J. Atmos. Sci.* **41**, 524–537.

GOTTLIEB, D. & ORSZAG, S. A. 1977 Numerical analysis of spectral methods: theory and applications. *NSF-CBMS Monograph no.* 26, Soc. Ind. App. Math.

GREENE, G. E. & HOOKE, W. H. 1979 Scales of gravity waves generated by instability in tropospheric shear flows. *J. Geophys. Res.* **84**, 6362–6364.

HARDY, K. R., REED, R. J. & MATHER, G. K. 1973 Observation of Kelvin–Helmholtz billows and their mesoscale environment by radar, instrumented aircraft, and a dense radiosonde network. *Q. J. R. Met. Soc.* **99**, 279–293.

HO, C.-M. & HUERRE, P. 1984 Perturbed free shear layers. *Ann. Rev. Fluid Mech.* **16**, 365–424.

KELLY, R. E. 1967 On the stability of an inviscid shear layer which is periodic in space and time. *J. Fluid Mech.* **27**, 657–689.

KELLY, R. E. 1968 On the resonant interaction of neutral disturbances in two inviscid shear flows. *J. Fluid Mech.* **31**, 789–799.

LAROCHE, H. 1987 Simulation numérique directe de couches de mélange en présence de rotation différentielle. Mémoire de DEA, Institut de Mécanique de Grenoble.

MCGOLDRICK, L. F. 1970 An experiment on second-order capillary gravity resonant wave interactions. *J. Fluid Mech.* **40**, 251–271.

MASLOWE, S. A. 1977 Weakly nonlinear stability theory of stratified shear flows. *Q. J. R. Met. Soc.* **103**, 769–783.

MASLOWE, S. A. 1986 Critical layers in shear flows. *Ann. Rev. Fluid Mech.* **18**, 405–432.

MASLOWE, S. A. & THOMPSON, J. M. 1971 Stability of a stratified free shear layer. *Phys. Fluids* **14**, 453–458.

METCALF, J. I. & ATLAS, D. 1973 Microscale ordered motions and atmospheric structure associated with thin echo layers in stably stratified zones. *Boundary Layer Met.* **4**, 7–36.

MILES, J. W. & HOWARD, L. N. 1964 Note on a heterogeneous shear flow. *J. Fluid Mech.* **20**, 331–336.

NAYFEH, A. H. 1973 Second-harmonic resonance in the interaction of an air stream with capillary–gravity waves. *J. Fluid Mech.* **59**, 803–816.

PATNAIK, P. C., SHERMAN, F. S. & CORCOS, G. M. 1976 A numerical simulation of Kelvin–Helmholtz waves of finite amplitude. *J. Fluid Mech.* **73**, 215–240.

RILEY, J. J. & METCALFE, R. W. 1980 Direct numerical simulation of a perturbed, turbulent mixing layer. *AIAA paper* 80-0274.

SCOTTI, R. S. & CORCOS, G. M. 1972 An experiment on the stability of small disturbances in a stratified free shear layer. *J. Fluid Mech.* **52**, 499–528.

STUART, J. T. 1971 Nonlinear stability theory. *Ann. Rev. Fluid Mech.* **3**, 347–370.

USHER, J. R. & CRAIK, A. D. D. 1975 (with an Appendix by F. Hendriks) Nonlinear wave interactions in shear flows. Part 2. Third-order theory. *J. Fluid Mech.* **70**, 437–461.

WOODS, J. D. 1968 Wave induced shear instability in the summer thermocline. *J. Fluid Mech.* **32**, 791–800.